Tectonophysics 746 (2018) 398–411

Contents lists available at ScienceDirect

Tectonophysics

journal homepage: www.elsevier.com/locate/tecto

Strength and elastic thickness variations in the Arabian Plate: A combination of temperature, composition and strain rates of the lithosphere

Magdala Tesauro [a,*], Mikhail K. Kaban [b], Alexey G. Petrunin [c,b], Sami El Khrepy [d,e], Nassir Al-Arifi [d]

[a] University of Utrecht, Utrecht, Netherlands
[b] German Research Centre for Geosciences (GFZ) Potsdam, Germany
[c] Faculty of Earth Sciences, Goethe University, Frankfurt am Main, Germany
[d] King Saud University, Riyadh, Saudi Arabia
[e] National Research Institute of Astronomy and Geophysics NRIAG, Helwan, Egypt

ARTICLE INFO

Article history:
Received 26 October 2016
Received in revised form 21 February 2017
Accepted 6 March 2017
Available online 9 March 2017

Keywords:
Arabian Plate
Lithospheric structure
Strain rate variations
Strength and effective elastic thickness of the lithosphere

ABSTRACT

The Arabian Plate shows a strong asymmetry between its Shield and Platform, in terms of topography, seismic velocity and density structure of the upper mantle. This asymmetry also results in significant rheological differences between these blocks, as revealed by the effective elastic thickness (EET) estimates, obtained using a spectral gravity method. However, these estimates may be biased due to various factors. Therefore, other approaches based on a direct rheological modeling of the lithospheric structure should be employed to verify these results. In this study, we use a recent model of the lithosphere, based on an integrative interpretation of the gravity field and seismic tomography, to correct an initial thermal model obtained from the inversion of seismic velocity, assuming a uniform composition. The results are used together with the most recent crustal model of the Arabian Plate to construct two alternative models of strength and EET of the lithosphere. The first model (Model I) assumes a constant value of 10^{-15} s^{-1} for the strain rates. In the second model (Model II), we used the strain rates obtained from a global mantle flow model. Model I confirms the asymmetry in the rigidity of the Shield and Platform. In contrast, Model II shows that the influence of the variable strain rates causes a significant increase in the strength and EET of the central and eastern part of the Shield and in contrast to previous studies, reveals that most of the Arabian Plate is a long-term stable tectonic feature, predominantly characterized by large EET values (≥70 km).

1. Introduction

The Arabian Plate is located in the center of the Middle East and is composed of the Arabian Shield in the west, uncovered by sediments and elevated up to 3000 m, and the Arabian Platform in the east, overlain by thick sediments (Fig. 1a). The strong asymmetry of the plate could be either the result of the lithospheric heterogeneity that occurred in the Neoproterozoic during its formation or the result of rifting forces acting along the Red Sea in the west and the Gulf of Aden in the south, as well as subduction of the Arabian lithosphere under Eurasia in the northeast (Stern and Johnson, 2010).

Seismic tomography models have also shown a strong difference between the upper mantle in the Shield and Platform. These features are characterized at a depth of 100 km by slow (4.1 km/s) and fast S-wave velocities (4.5 km/s), indicating a sharp increase in the lithospheric thickness from the Shield (80–90 km) to the Platform (160–200 km) (Park et al., 2007; Hansen et al., 2008; Chang et al., 2011; Schaeffer and Lebedev, 2013). These results, as well as the mantle temperatures determined from xenoliths (McGuire and Bohannon, 1989), point to the presence of partial melt (between 4 and 10% according to Camp and Roobol, 1992) and in general to an upper mantle that is hotter in the western part of the Arabian Plate, than in the eastern part. This is also in agreement with recent volcanic activity, which affects a wide region of western Arabia, from eastern Yemen to Saudi Arabia, Jordan, and Syria. The increase in seismic velocities further in the northeast is related to the continental collision. Kaban et al. (2016a) have recently shown that these parts of the Arabian Plate also have a different density structure: the Arabian Shield is relatively dense up to a depth of ~80 km, likely due to a phase of metasomatic refertilization that occurred at ~800 Ma, due to mantle upwelling (Stern and Johnson, 2010; O'Reilly and Griffin, 2012). Below this depth, the upper mantle has low density, probably associated with the hot upwelling mantle, which is connected to the low-density conduit under the Red Sea. The uppermost mantle in the central part of the Platform has a somewhat low density, likely due to the depletion of high-density constituents (e.g., Priestley et al., 2012),

* Corresponding author.
E-mail address: magdala@gfz-potsdam.de (M. Tesauro).

http://dx.doi.org/10.1016/j.tecto.2017.03.004
0040-1951/

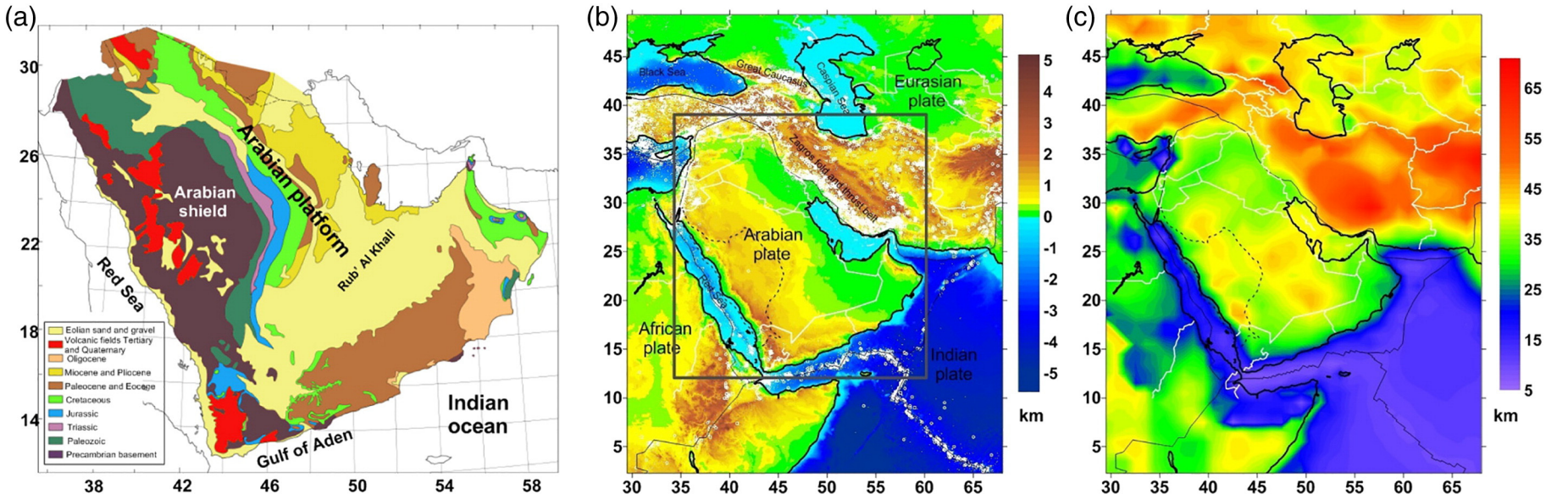

Fig. 1. (a) Geological map of the Arabian Plate. (b) Topography of the study area. White circles show earthquake locations. The rectangle outlines the study area. (c) Moho depth (Kaban et al., 2016a). Thin grey contours show the main plate boundaries. White contours show state boundaries. The dashed black contour shows the boundary between the Arabian Shield and Platform.

while the lower part has a relatively high density up to a depth of ~200 km (bottom of the lithosphere).

The difference in the lithospheric structure and composition results in variations in the rigidity of the lithosphere. Tesauro et al. (2012a), showed that the effective elastic thickness (EET) values, based on the strength distributions (Tesauro et al., 2012b), are only partly consistent with those based on a cross–spectral analysis of the gravity data (Audet and Bürgmann, 2011). Furthermore, the spectral method usually does not show a sharp transition between adjacent tectonic features that significantly differ in temperatures and lithospheric thickness. For this reason, these estimates do not have a bimodal distribution like those obtained from a rheological approach, but tend to be distributed more uniformly. On the other hand, the EET estimated from strength distributions is affected by uncertainties in the input parameters (e.g., thermal model, rheological laws and parameters), while those obtained from spectral gravity methods may have large uncertainties in presence of flat topography (Tesauro et al., 2012a). Based on the above discussion, we can conclude that the EET needs to be estimated using different approaches and more constraints on the initial data for a more realistic assessment of the rheological properties and rigidity of the lithosphere.

In the recent thermo-rheological models of the lithospheric strength and EET, uncertainties in the input thermal model have been reduced, by taking into account the effects of compositional variations in the upper mantle, which were determined by a joint inversion of seismic tomography and gravity data (e.g., Tesauro et al., 2015). Furthermore, Tesauro et al. (2013) discussed the effect of the crustal rheology on the strength/EET using end-member 'hard' (HRM) and a 'soft' (SRM) rheology models for the continental crust. They found that rheological variations cause significant changes in the integrated strength/EET distribution in the areas characterized by intermediate thermal conditions. However, these studies still employed a constant value for the strain rates (10^{-15} s^{-1}), which could significantly affect the results (Tesauro et al., 2015). Global models of strain rates, constrained by geodetic determinations of plate velocities, indicate that this parameter may vary by several orders of magnitude depending on the tectonic activity of the area (e.g., Kreemer et al., 2014). The tests performed by varying the strain rates by one order of magnitude have demonstrated that the strength may change significantly within the cratons (Tesauro et al., 2015). For the first time, we use recent estimates of the strain rates, varying both horizontally and with depth, obtained from global dynamic models of the mantle (Petrunin et al., 2013; Kaban et al., 2014) to evaluate this effect on the predicted EET.

In this study, we also use a recent detailed model of the crust and upper mantle of the Middle East (Kaban et al., 2016a) to derive the physical parameters of the lithosphere (e.g., density and thickness of the lithospheric layers) and surface heat flow measurements in the Arabian Plate to constrain the crustal temperatures. The temperatures in the upper mantle were initially estimated by inverting the seismic tomography model SL2013sv of Schaeffer and Lebedev (2013), assuming a uniform composition. Afterwards, this initial temperature distribution was corrected for compositional variations and small-scale details using the high-resolution density model of Kaban et al. (2016a). The new thermal field and recent crustal model of the Middle East of Kaban et al. (2016a, 2016b) provide the input for the models of strength and EET. The first set of models were obtained using a constant average value for the strain rates, while in the second one we took into account variations of the strain rates, according to a numerical model. We discuss the results in comparison with the EET estimates of Chen et al. (2015), which are based on the cross-spectral method. This analysis provides a better understanding of the two main tectonic features of the Arabian Plate.

2. Thermal model

The thermal structure of the internal part of the Arabian Plate is poorly constrained, since very little heat flow (HF) data are available (Fig. 2). The HF measurements conducted at four sites in Saudi Arabia by Gettings et al. (1986) give values in the range of 35–44 mW m^{-2}. Larger values have been determined in the peripheral parts of the Arabian Plate, such as in Oman (44 ± 4 mW m^{-2}, Rolandone et al., 2013) and in Jordan, where Galanis et al. (1986) estimated HF in the range of 42–65 mW m^{-2}, and more recently, Förster et al. (2010) provided an average of 60 mW m^{-2}. On the other hand, there exist many measurements in the HF in the Red Sea and Gulf of Aden, indicating an increase of the HF toward the western and southwestern border of the Arabian Plate, up to 90 mW m^{-2} within a distance of 40–50 km on the Red Sea flanks, while they remain relatively low in the eastern Gulf of Aden (45 mW m^{-2}) (Rolandone et al., 2013). Therefore, the relatively low HF values in the Arabian Shield is inconsistent with both surface and body wave tomography (e.g., Park et al., 2007; Koulakov et al., 2016), which suggest that the mantle lithosphere beneath the Arabian Shield is thin and hot.

To construct a 3D thermal model of the lithosphere, we first extrapolated the surface HF values on a regular grid (1° × 1°) covering the entire Arabian Plate, based on the existing surface HF data (http://www.heatfow.und.edu/, Fig. 2). We assumed a value of 40 mW m^{-2} for most of the Arabian Platform. In contrast, the HF gradually increases to the west of the Shield and along the southern margin of the Platform up to 100 mW m^{-2} in the Red Sea and western part of the Gulf of Aden and up to 60 mW m^{-2} in the eastern part of the Gulf of Aden, consistent with existing data (Fig. 2). Afterwards, we used the continental geotherms of Hasterok and Chapman (2011) to determine the temperature in the crust. These authors computed geotherms for different values of the surface HF using a heat production model based on the petrology of the crust and mantle and incorporating thermal conductivity results from recent laboratory measurements.

For the upper mantle, initial temperature variations at depths from 100 km to 300 km were estimated by inversion of the recent S-wave model SL2013sv of Schaeffer and Lebedev (2013). For this purpose, we used the mineral physics approach of Stixrude and Lithgow-Bertelloni (2005) and the anelasticity model of Cammarano et al. (2003). In the inversion, a uniform "fertile" composition was initially adopted, which is defined as an average of the mineral fractions constituting the "Primitive mantle" rock (McDonough and Sun, 1995) and the "Tecton garnet peridotite" rock (Griffin et al., 2003): Ol: 58.5%, OPX:

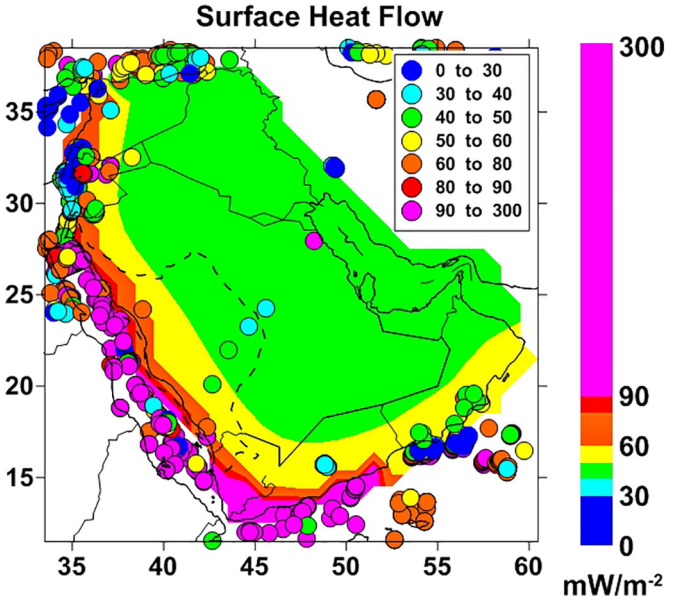

Fig. 2. Surface heat flow map. The values have been estimated using surface heat flow data (http://www.heatfow.und.edu/) as constraints and are displayed by color filled circles. Continuous black contours show state boundaries. The dashed black contour shows the boundary between the Arabian Shield and Platform.

15%, CPX: 11.5%, and Gt: 15%, with a Mg# (100 x Mg/(Mg + Fe)) = 89. In the uppermost part of the mantle (between 100 km and the Moho depth) temperatures were linearly interpolated to those estimated in the crust, to ensure a smooth transition between the two models. As a result, a strong difference at a depth of 100 km is found between the hot Arabian Shield, characterized by temperatures of ~1300 °C and the Arabian Platform, where the temperatures decrease to ~900 °C. The coldest regions (~750 °C) are the western border of the Zagros Mountains and Arabian Gulf, farther to the east, which reflect the presence of the subducting slab (Fig. 3a).

As reported by Schaeffer and Lebedev (2013), the horizontal resolution of the tomography model SL2013sv does not exceed 4–5° (450–550 km), which is insufficient for this regional study. Therefore, we used the density model of Kaban et al. (2016a), with a horizontal resolution of about 150 km, in which the resolution of the initial density model obtained from the inversion of Schaeffer and Lebedev (2013) was improved using gravity data. In the last study, the residual mantle gravity anomalies and residual topography were estimated by removing the effect of the crust and that of the deep mantle from the observed fields. Therefore, the residual fields show the effect of density variations in the upper mantle. The residual gravity and residual topography have been jointly inverted using an initial density model depending only on the thermal field described above. In the Occam type inversion, the initial model has been modified to fit both the residual mantle gravity field and residual topography (see for technical details, Kaban et al., 2016a). This inversion significantly improves the resolution of the upper mantle structure, in particular by localizing the features smeared in the tomography model. The final model also reflects possible variations of composition not well-resolved by the seismic tomography.

The final density variations from Kaban et al. (2016a) have been converted into temperatures (Fig. 5a and b) using a polynomial function fitting these two parameters at different depths, estimated using a uniform "fertile" upper mantle composition (Fig. 4). The changes at a depth of 100 km beneath the Shield and Platform, in comparison with the

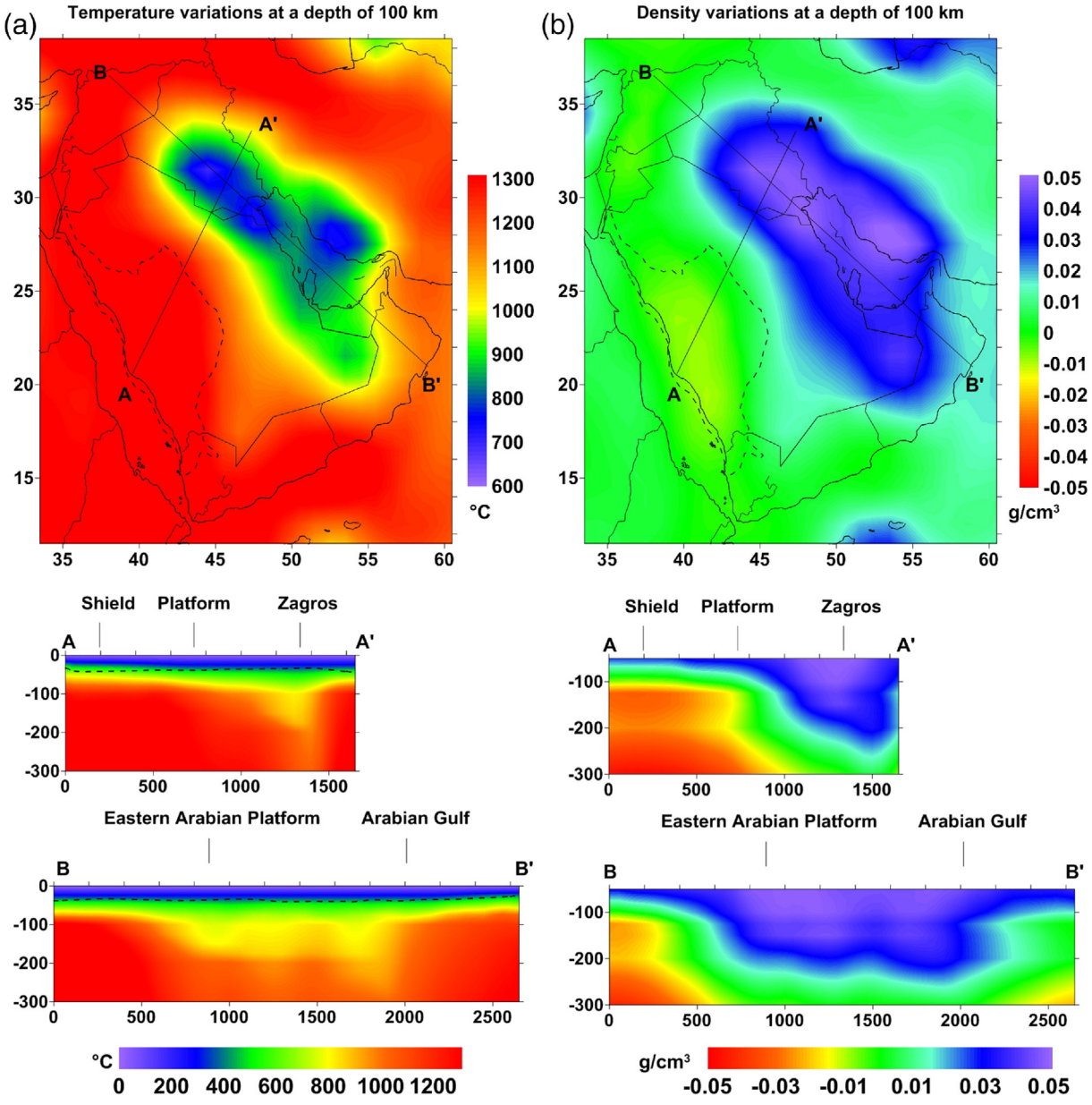

Fig. 3. Initial (a) temperature and (b) density variations. Both fields are displayed at a depth of 100 km (Kaban et al., 2016a), and along two cross-sections (A-A′ and B-B′, respectively), estimated assuming a "fertile" upper mantle composition. Horizontal and vertical axes of the cross-sections display the distance and depth (both in km), respectively. Locations of the cross-sections are shown by the two black lines. Continuous black contours show state boundaries. The dashed black contour shows the boundary between the Arabian Shield and Platform.

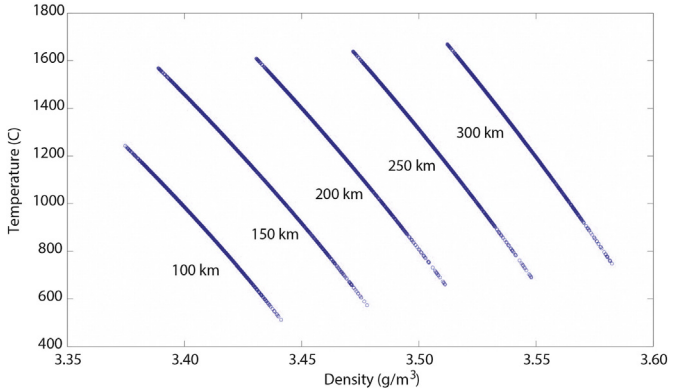

Fig. 4. Relationship between temperature and density variations, assuming a "fertile" upper mantle composition. See text for further explanations.

initial density model (Figs. 3b and 5a, and cross-sections A-A′ and B-B′), leads to a reduction of the difference in temperatures between these two tectonic features of about 100–200 °C (Fig. 5a and cross-sections A-A′ and B-B′). At greater depths (>200 km) the increase of density in the final model beneath the western margin of the Zagros Mountains, reflecting the subduction of the slab (Fig. 5a, cross-sections A-A′), causes only a moderate temperature decrease (~50 °C). The final thermal model was used for estimations of the strength and EET of the lithosphere.

3. Methods

3.1. Strength and effective elastic thickness

The final density and thermal field (Fig. 5a and b), together with the crustal model of Kaban et al. (2016a), are used as the main input for calculation of the lithosphere strength. The model of Kaban et al. (2016a) provides the physical properties of the sediments and three layers of

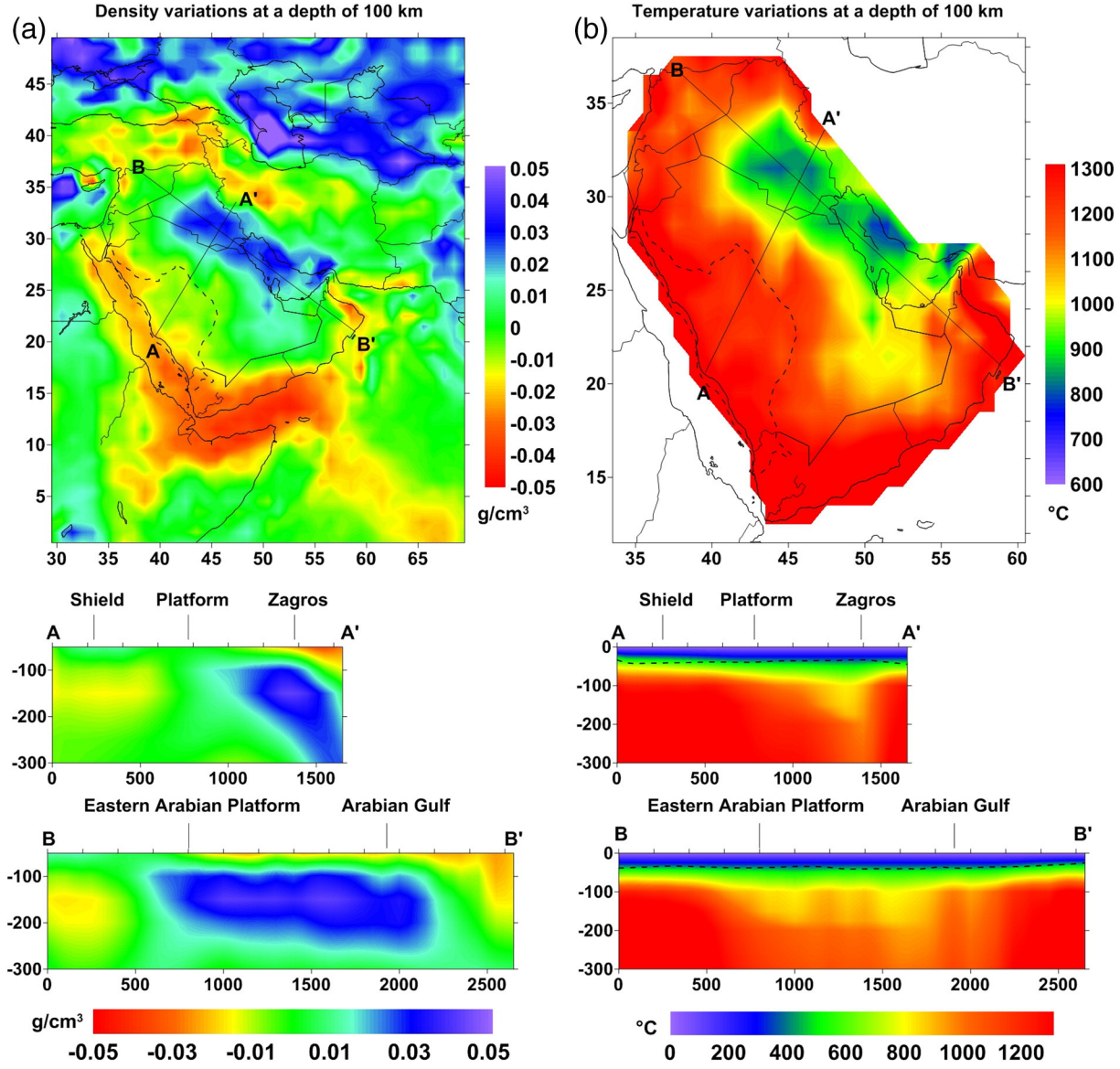

Fig. 5. Corrected (a) density and (b) final temperature variations. Both fields are displayed at a depth of 100 km and along two cross-sections (A-A′ and B-B′, respectively). Horizontal and vertical axes of the cross-sections display the distance and depth (both in km), respectively. Locations of the cross-sections are shown by the two black lines. Continuous black contours show state boundaries. The dashed black contour shows the boundary between the Arabian Shield and Platform.

the crystalline crust (Fig. 1c) Stolk et al. (2013), which is based on the most complete seismic dataset, compiled by the US Geological Survey (Mooney, 2014), and uses a robust interpolation methodology. For marginal areas, uncovered by the model of Kaban et al. (2016b), the global model CRUST1.0 (Laske et al., 2013) is employed. We used the relationship of Christensen and Mooney (1995) to convert the crustal velocities in densities, while in the sediments we estimated the average density value among those characterizing each basin (Stolk et al., 2013).

The integrated lithospheric strength (σ_L) is estimated by vertical integration of the yield strength envelope (YSE), which predicts the maximum differential stress required to the rocks before failure (Goetze and Evans, 1979):

$$\sigma_L = \int_0^h (\sigma_1 - \sigma_3) dz \quad (1)$$

where h is the lithospheric thickness and σ_1 and σ_3 are the maximum and minimum principal stresses, respectively.

The crustal rocks can be deformed in the brittle or ductile conditions. The brittle condition may be approximated by Byerlee's law (Byerlee, 1978):

$$\sigma_b = f\rho g z(1-\lambda) \quad (2)$$

where $\sigma_b = \sigma_1 - \sigma_3$ is the friction-related differential stress, f is a dimensionless parameter depending on the frictional coefficient and deformational regime, ρ is the density, g is the acceleration of gravity, z is the thickness of each lithospheric layer, and λ is the pore fluid factor.

The power-law dislocation creep, describing the ductile deformation of the crustal ductile strength (σ_d), is estimated according to Goetze and Evans (1979):

$$\sigma_d = \left[\frac{\dot{\varepsilon}}{A_P}\right]^{\frac{1}{n}} \cdot \exp\left[\frac{E_P}{nRT}\right] \quad (3)$$

where $(\sigma_d) = \sigma_1 - \sigma_3$ is the ductile-related differential stress, $\dot{\varepsilon}$ is the strain rate, A_P is the power strain rate, n is the power law exponent, E_P is the power law activation energy, R is the gas constant, and T is the temperature.

The high crustal velocities of the Arabian Plate, estimated by Stolk et al. (2013), indicate a predominantly mafic crustal composition. Therefore, we associate a stiff rheology, corresponding to that of "dry granite", "felsic granulite", and "dry diabase" to the upper, middle, and lower crust, respectively. At high stress and relatively low temperatures (<1000 °C), characterizing the uppermost mantle, rocks deform in ductile conditions according to the Dorn law. We used the results of the most recent laboratory experiments that have derived the exponential flow law for a "dry olivine" (Eq. (4)), applicable to the uppermost mantle (Demouchy et al., 2013).

$$\sigma_d = \sigma_D \left(1 - \left[-\frac{RT}{E_D} \cdot \ln\left(\frac{\dot{\varepsilon}}{A_D}\right)\right]^{1/2}\right)^2 \quad (4)$$

where σ_D is the Dorn law stress, E_D is the Dorn law activation energy, and A_D is the Dorn law strain rates.

In order to assess the effect of the strain rates variations on the lithospheric strength, we first adopted in the calculations a uniform value for the strain rates of 1×10^{-15} s^{-1}, already used in previous studies (Tesauro et al., 2015). We then repeated the calculations by employing the estimated strain rate variations, using the global mantle convection model as described in Section 3.2. The rheological parameters are displayed in Table 1.

Based on the YSEs of both strength models (fixed and variable strain rates) the thickness of the mechanically strong part of the lithospheric layer, which extends from the top of the layer to the depth of a specific temperature (e.g., 350 °C for quartzite), at which the yield stress is below a threshold of 10 MPa (e.g., Ranalli, 1994), has been computed. According to Burov and Diament (1995), the lithospheric layers are coupled or decoupled depending on the strength relative to this predefined threshold. Following this approach, we estimated the EET as a function of the thickness of the mechanically strong layers (Δh_i), for the coupled (5) and decoupled (6) conditions.

$$T_e^{(n)} = \left(\sum_{i=1}^{n} \Delta h_i\right) \quad (5)$$

$$T_e^{(n)} = \left(\sum_{i=1}^{n} \Delta h_i^3\right)^{1/3} \quad (6)$$

In the calculation, we took into account variations of the Young's Modulus with depth (Tesauro et al., 2015) not considered in Burov and Diament (1995).

3.2. Strain rate variations in the lithosphere

As discussed in the previous section, ductile deformation controlled by dislocation creep and low temperature plasticity depends on strain rates. Estimates of lateral and vertical variations of this parameter are fundamental for a robust calculation of the YSEs. Since plate tectonics are driven by many forces including large-scale mantle flows, only a global mantle convection model can provide these estimates. The model has to include rigid plates, weak plate boundaries, realistic densities and a viscosity distribution for the entire mantle and crust. The

Table 1
Rheological model parameters.

Parameter	Symbol	Units	Sediments	Upper crust	Middle crust	Lower crust	Upper mantle
Composition	–	–	–	Granite (dry)[a]	Felsic Granulite[b]	Diabase (dry)[a]	Olivine PL(dry)[c] Olivine DL(dry)[d]
Density min-max/mean	ρ	km/m^{-3}	1900–2670/2424	2558–2957/2796	2741–3041/2904	2865–3251/3077	3364–3493/3406
Layer thickness min-max/mean	z	km	0–21/3.1	0–23.5/8.4	0.5–29.5/10.2	0.5–27.5/10.2	34–293/135
Friction coefficient extensional/compressional conditions	f	–	0.75/3	0.75/3	0.75/3	0.75/3	0.75/3
Pore fluid factor	λ	–	0.36	0.36	0.36	0.36	0.36
Power law exponent	n	–	–	3.3	3.1	3.05	3
Power law activation energy	Ep	kJ mol^{-1}	–	186	243	276	510
Power law strain-rate	A_p	Pa^{-n} s^{-1}	–	3.16×10^{-26}	2.01×10^{-21}	6.31×10^{-20}	1.2589×10^{-12}
Dorn law activation energy	E_D	kJ mol^{-1}	–	–	–	–	450
Dorn law strain-rate	A_D	s^{-1}	–	–	–	–	1.0×10^{6}
Dorn law stress	σ_D	Pa	–	–	–	–	15×10^{9}
Strain rate	ε	s^{-1}	–	10^{-15}	10^{-15}	10^{-15}	10^{-15}

[a] Carter and Tsenn (1987).
[b] Wilks and Carter (1990).
[c] Karato and Jung (2003).
[d] Demouchy et al. (2013).

resulting plate velocities are constrained by the observed GPS data. However, the GPS stations are mainly located along the boundaries of the Arabian Plate (e.g., ArRajehi et al., 2010) and thus do not provide proper constraints for the entire plate. Therefore, we used the plate velocity model NRR-MORVEL56 (Argus et al., 2011) that provides homogeneous coverage of the whole area. To calculate present-day mantle flow velocities, we solve the Navier-Stokes equation together with the Poison equation satisfying the momentum and mass conservation conditions. The numerical code ProSpher is employed to estimate mantle flow velocities (Petrunin et al., 2013; Kaban et al., 2014). The ProSpher code combines the advantages of both spectral-based and FD/FE methods, providing a way to account for strong lateral viscosity variations (up to 5 orders of magnitude laterally), self-gravitation and compressibility.

Density variations in the lower mantle and in the upper mantle outside the study area are calculated using the velocity-to-density scaling factor of 0.28 (Steinberger and Calderwood, 2006) and the S-velocity tomography model S40RTS (Ritsema et al., 2011), for depths > 300 km, and the SL2013sv (Schaeffer and Lebedev, 2013) for the shallower layers. For the Arabian Plate and its surroundings, the results from Kaban et al. (2016b) are used for the upper mantle density variations. The viscosity distribution is considered as a combination of the radial and lateral deviation components. The radial component is given by the radial-dependent viscosity profile from Steinberger and Calderwood (2006). The lateral variation of viscosity is calculated using the so-called homologous temperature approach (e.g., Paulson et al., 2005) taking into account the temperature distribution in the mantle. Plate boundaries and weak zones within the lithosphere are introduced by converting the integrated Global Strain Rate Model (GSRM) (Kreemer et al., 2014) into the effective viscosity for the upper 100 km of the lithosphere. The full method and setup are described in detail in Petrunin et al. (2013) and Kaban et al. (2015). An appropriate fit of the calculated surface velocities and the plate velocity model NRR-MORVEL56 (Argus et al., 2011) is achieved by varying the free coefficients in the formulas for the temperature-to-viscosity transformation and the effective viscosity at weak plate boundaries (Kaban et al., 2014). Finally, the resulting velocity vector field is transformed into a 3-D distribution of the second invariant of the strain rate tensor. Variations of this field at a depth of 100 km and along two cross-sections (Fig. 6) show a distinct difference in the rate of deformation between the western and eastern parts of the Arabian Plate. At a depth of 100 km, the strain rates are decreasing by three orders of magnitude from the Shield to Platform. According to previous studies (Chang et al., 2011), the hot and low-viscous mantle flow moves from the Afar plume to Lebanon just beneath the Shield, transmitting stress and additional heat flux to the lithosphere of the Shield, which makes its viscosity less than that of the Platform. In turn, the colder Platform has a higher rigidity, which is expressed by significantly lower strain rates (cross-sections A-A′ and B-B′, Fig. 6).

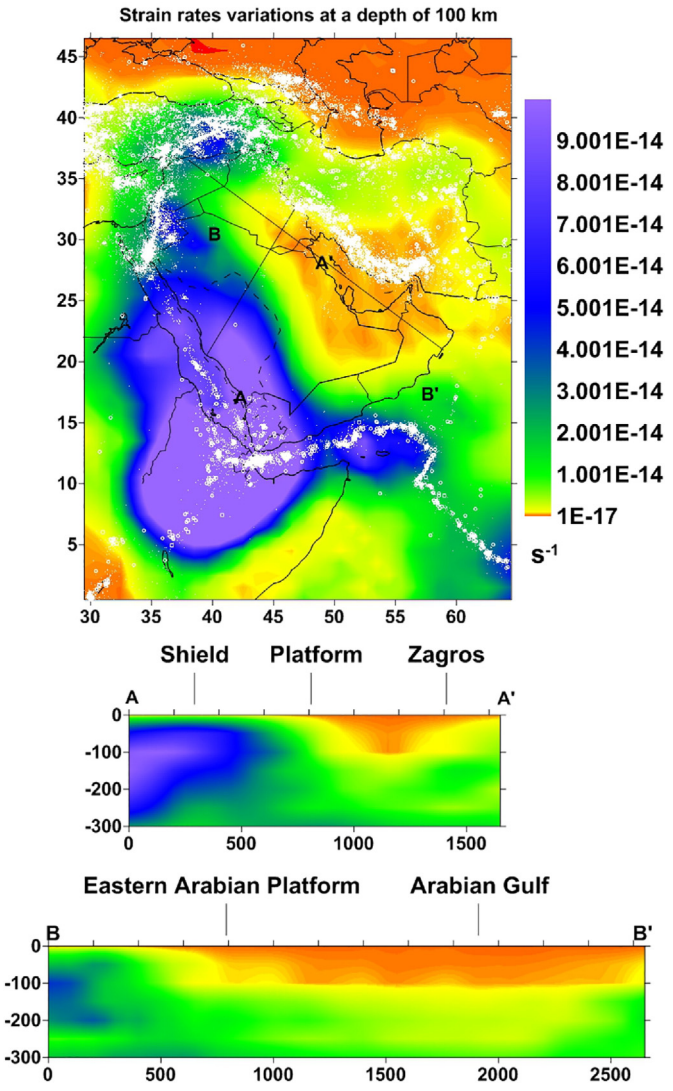

Fig. 6. Variations of the second invariant of the strain rate tensor at a depth of 100 km and along two cross-sections (A-A′ and B-B′, respectively). Horizontal and vertical axes of the cross-sections display the distance and depth (both in km), respectively. Locations of the cross-sections are shown by the two black lines. Continuous black contours show state boundaries. The dashed black contour shows the boundary between the Arabian Shield and Platform. White circles show the earthquakes location.

4. How strong is the Arabian Plate?

The results in terms of the integrated lithospheric strength, the percentage of the crustal strength with respect to the total value for the entire lithosphere, strength variations along three cross-sections, and three YSEs for key tectonic features, are displayed for Model I (fixed strain rates) in Figs. 7 and 9 and Model II (variable strain rates) in Figs. 8 and 10. Model I shows a sharp increase in the strength from the Shield to the Platform (Figs. 7a, cross-section A-A′ and 4a). This increase is mostly due to temperature variations (Fig. 5b), primarily in the mantle lithosphere, since the crustal thickness is rather uniform. Therefore, we have a distinct difference in strength between these two tectonic units, with the largest values estimated in the northeastern part of the Platform. However, the strength remains concentrated in the crust (>70%) both in the Shield and Platform, (Figs. 7b–c, cross-section A-A′ and B-B′). The only region in which the strength is almost equally partitioned between the crust and mantle lithosphere is the easternmost part of the Platform, close to the Zagros Mountains, due to the cold subducting lithosphere (Figs. 7b–c and Fig. 7a, cross-sections A-A′ and C-C′). Therefore, throughout the entire Arabian Plate, the strength is apparently distributed according to the crème brulée model, implying a relatively strong crust underlain by a weak mantle (e.g., Jackson, 2002). If this is the case, the region should not be stable on a long-term time scale (e.g., François et al., 2013).

On the other hand, when we take into account the lateral variations of the strain rates (Model II), the strength pattern changes significantly (Fig. 8a–c). In particular, the increase in the strain rates as high as 10^{-13} s^{-1} in the western part of the Arabian Plate, and the decrease as high as 10^{-17} s^{-1} in the southeastern part in the shallow upper mantle (50–100 km), reduces the difference in strength between these regions. The weakest part of the plate is limited to its western border, as the effect of high temperatures is partially compensated by the high strain rates in other parts of the Shield (Fig. 8a). This partial compensation causes an increase in the strength of the lithospheric mantle of the Shield by ~20% (Fig. 8b–c). The largest strength values are again estimated in the northeastern part of the plate, since the strain rates in

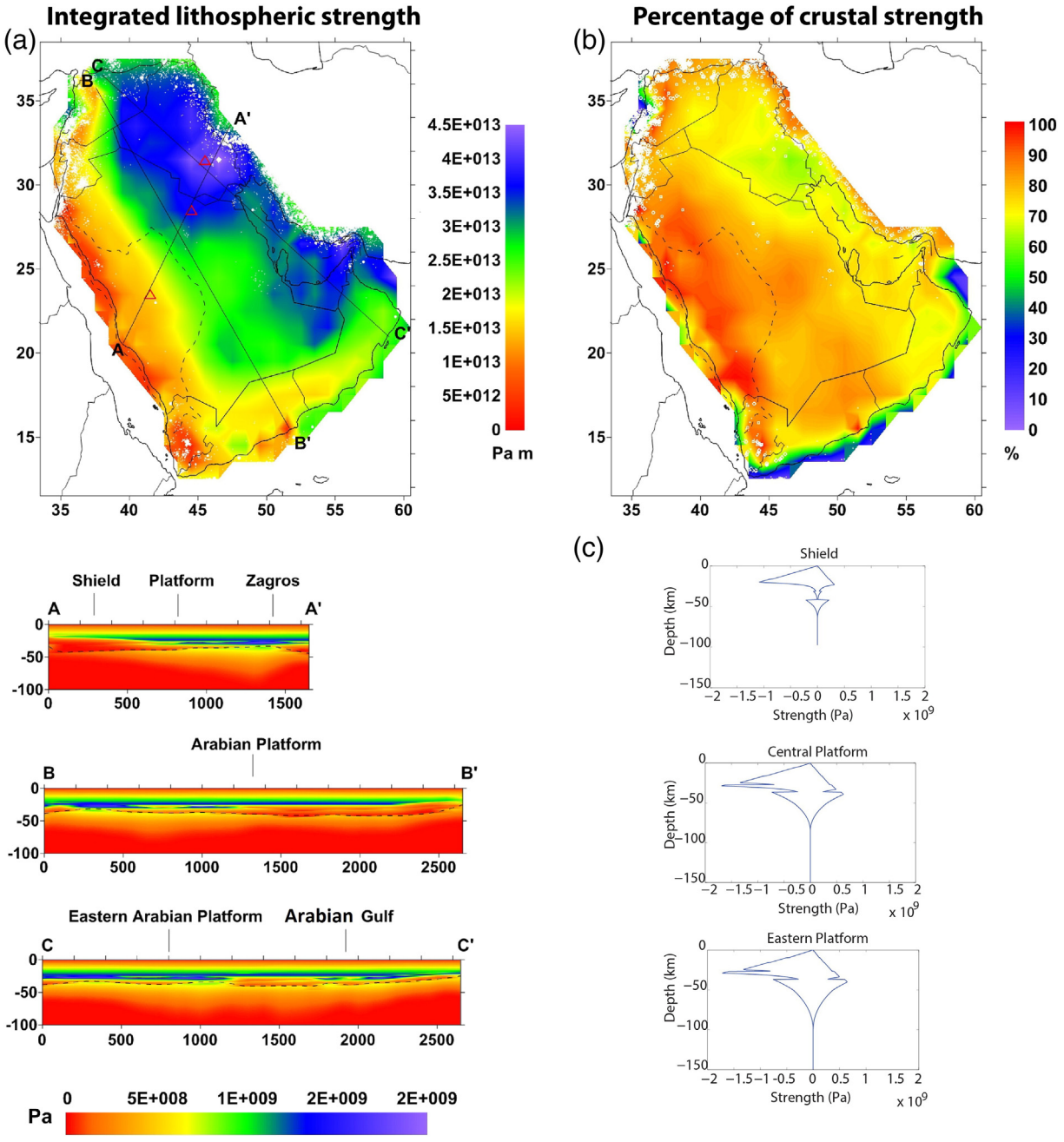

Fig. 7. Results for Model I: (a) Integrated strength and strength variations along three cross-sections (A-A′, B-B′, and C-C′, respectively) for compressional conditions. Horizontal and vertical axes of the cross-sections display the distance and depth (both in km), respectively. Location of the cross-sections is shown by the three black lines. (b) Percentage of crustal strength. (c) Yield strength envelopes (YSEs) of key tectonic features of the Arabian Plate. For convention, the values estimated under compressional and extensional conditions are shown as negative and positive, respectively. YSE locations are indicated by open red triangles displayed in panel a. Continuous black contours show state boundaries. The dashed black contour shows the boundary between the Arabian Shield and Platform. White circles show the earthquake locations.

Model II have similar values to those used in Model I. Notably, the large strength values are extended along the entire border of the Shield and are mainly concentrated in the northeastern part of the Platform (Fig. 8a). Furthermore, in Model II the strength is localized predominantly in the crust (60%–80%) in the entire plate, but with fewer lateral variations (Fig. 8b).

We can observe that in Model I, the thickness of the mechanically strong upper mantle (MSUM) is <20 km in the Shield, while it is increased in the Platform, reaching ~50 km in the easternmost part (Fig. 9a). The weakest regions, where the MSUM is almost absent, are the western and southwestern margins of the Arabian Plate, close to the rifting areas (Fig. 9a, cross-section A-A′). Furthermore, the crust is decoupled from the upper mantle in most of the Shield, while in the other parts of the Arabian Plate all the lithospheric layers are coupled (Fig. 9b). Both the coupling conditions and the relatively large thickness of the MSUM support the hypothesis that the Arabian Platform is stable, despite its strength is mainly confined to the crust (Figs. 7b). In contrast, the hot mantle lithosphere beneath the Shield and some peripheral parts of the Platform makes these features prone to deformation, similar to the tectonically active structures of the Phanerozoic age (e.g., the North American Cordillera, Tesauro et al., 2015). The changes of the coupling/decoupling conditions cause large differences in the EET, which ranges between 20 and 40 km in the Shield, with the lowest values corresponding to the western and southwestern margins, due to the high

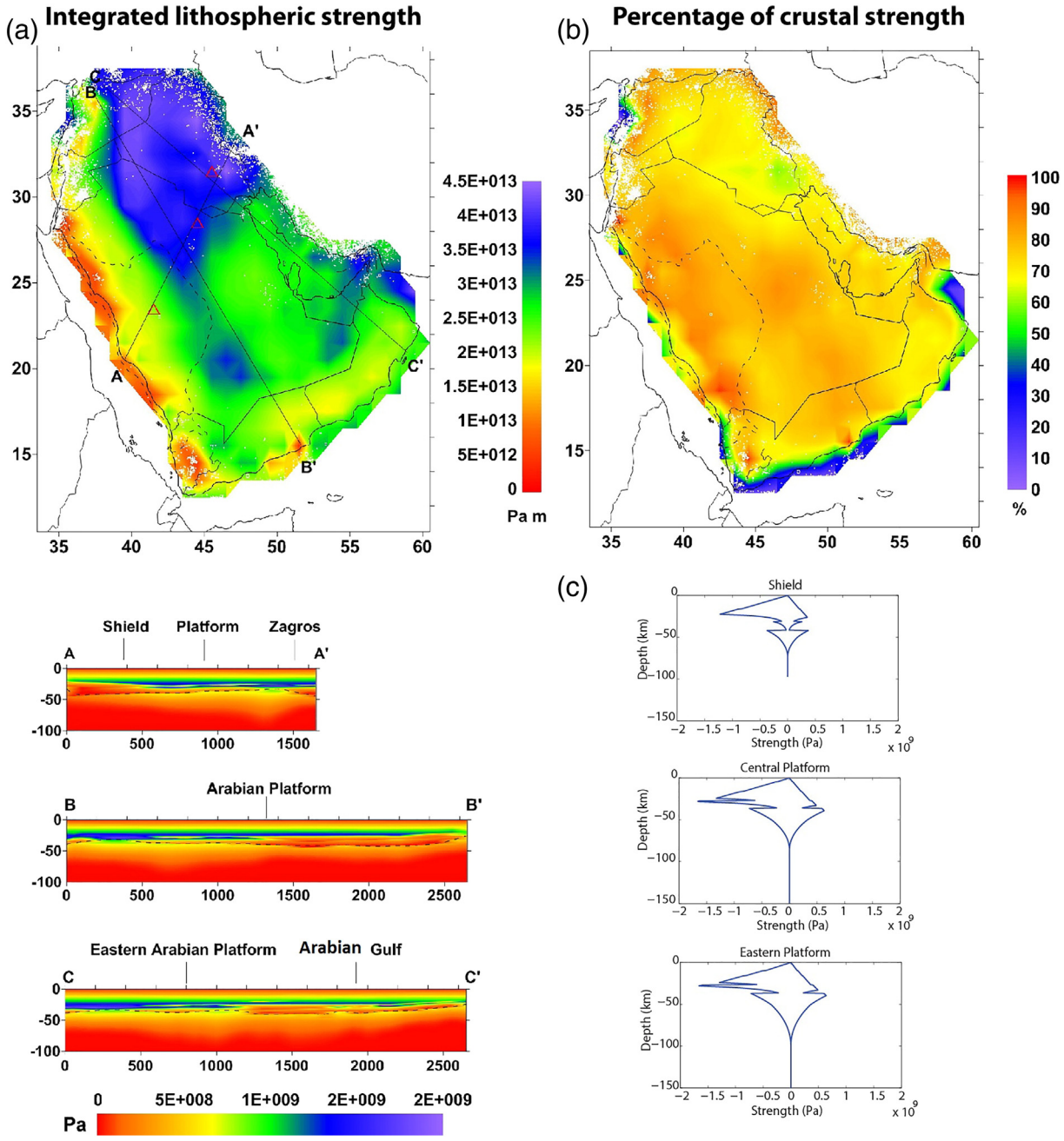

Fig. 8. Results for Model II: (a) Integrated strength and strength variations along three cross-sections (A-A′, B-B′, and C-C′, respectively) for compressional conditions. Horizontal and vertical axes of the cross-sections display the distance and depth (both in km), respectively. Location of the cross-sections is shown by the three black lines. (b) Percentage of crustal strength. (c) Yield strength envelopes (YSEs) of key tectonic features of the Arabian Plate. For convention, the values estimated under compressional and extensional conditions are shown as negative and positive, respectively. YSE locations are indicated by the open red triangles displayed in Fig. 8a. Continuous black contours show state boundaries. The dashed black contour shows the boundary between the Arabian Shield and Platform. White circles show the earthquake locations.

temperatures. In contrast, the EET sharply increases to 70 km close to the eastern border of the Shield, reaching the largest values (~100 km) near the Zagros Mountains and Arabian Gulf (Fig. 9c). The EET does not change significantly in the central part of the Platform, spanning from 60 km to 80 km (Fig. 9c), despite the decrease in strength and thickness of the MSUM from north to south (Fig. 7a cross section B-B′, and Fig. 9a). In Model II, the lateral variation in the strain rates does not influence significantly the thickness of the MSUM in the Platform (Fig. 10a), while causing an increase in the same parameter as high as 30 km in the eastern part of the Shield and coupling of all the lithospheric layers in almost the entire plate (Fig. 10b). Consequently, the EET is low (<40 km) only near to the Red Sea. It smoothly increases from 70 km to 80 km from the western to the eastern part of the Shield, while remaining unchanged in the Platform (Fig. 10c).

It has been demonstrated that the intraplate regions, dividing blocks with substantially different lithosphere strength (e.g., craton and off-craton regions), are characterized by increased seismic activity (Tesauro et al., 2015; Mooney et al., 2012). In the Middle East, seismicity occurs mainly along the plate boundaries surrounding the Arabian Plate (Figs. 1, 6, 7–10). The tectonic activity is primarily confined to the Red Sea axial rift, due to the extensional forces associated with strike-slip faults, lithosphere stretching, and thinning along the western margin

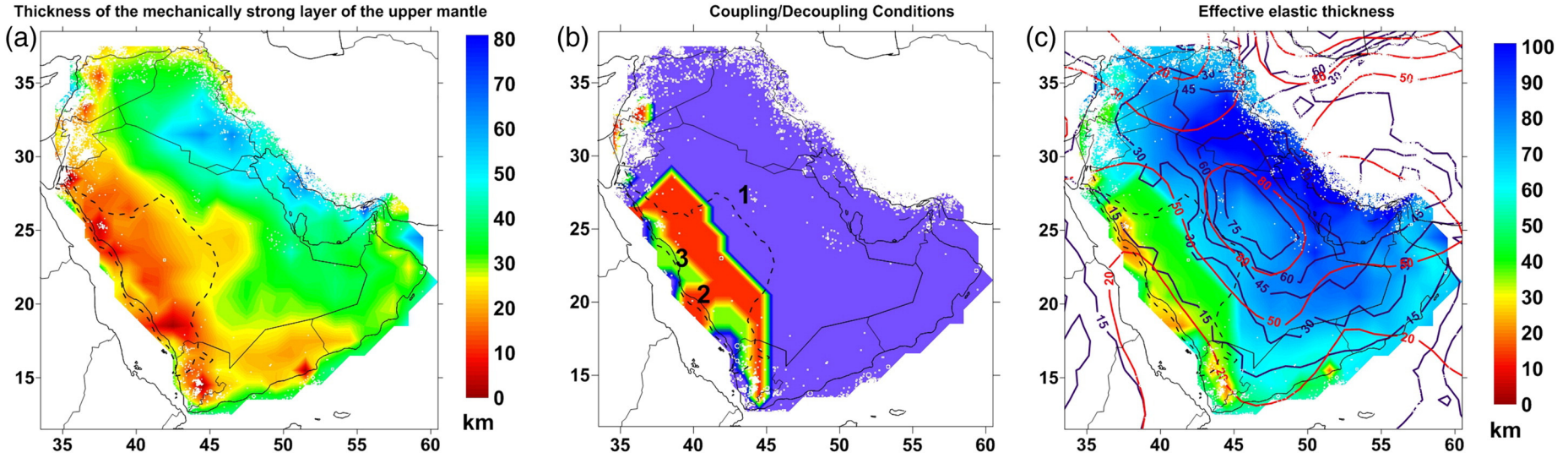

Fig. 9. Results for Model I: (a) Thickness of the mechanically strong layer of the upper mantle. (b) Coupling/decoupling conditions. Numbers indicate the following: 1. All the lithospheric layers are coupled. 2. Upper and middle crusts are coupled and all the other layers are decoupled. 3. Middle and lower crusts are coupled and all the other layers are decoupled. (c) Effective elastic thickness (EET). Violet and red contours with labels show the EET values from Audet and Bürgmann (2011) and Chen et al. (2015), respectively. Continuous black contours show state boundaries. The dashed black contour shows the boundary between the Arabian Shield and Platform. White circles show the earthquake locations.

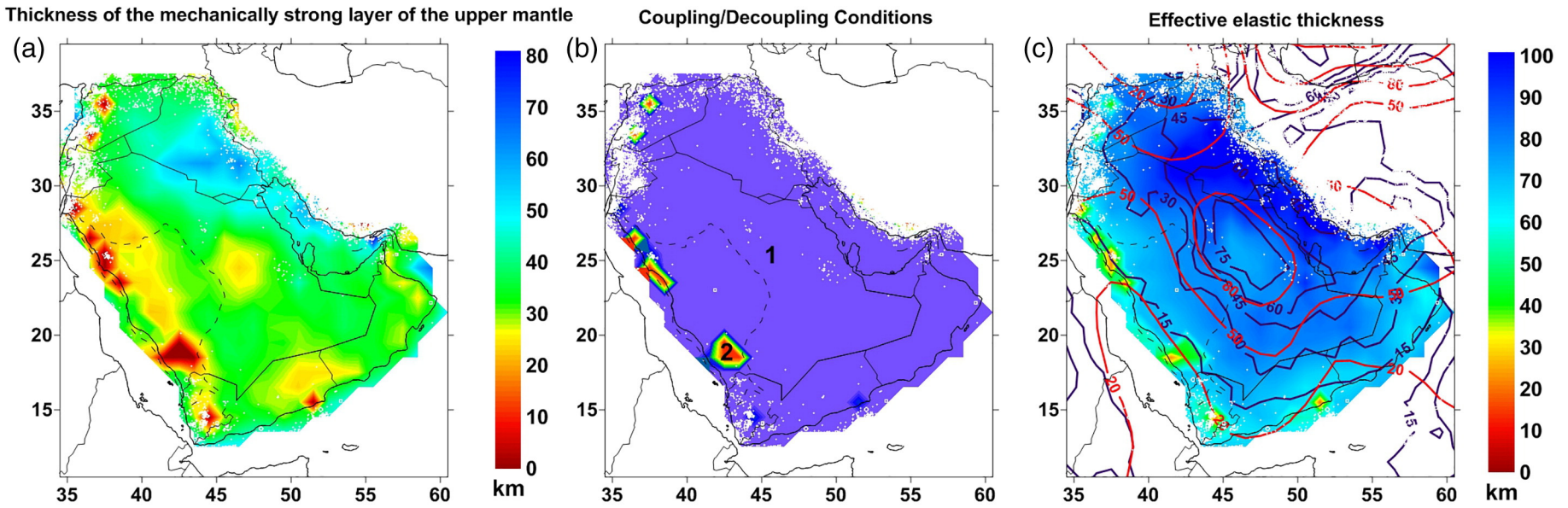

Fig. 10. Results for Model II: (a) Thickness of the mechanically strong layer of the upper mantle; (b) Coupling/decoupling conditions. Numbers indicate the following: 1. All the lithospheric layers are coupled. 2. Upper and middle crustal layers are coupled and all the other layers are decoupled. (c) Effective elastic thickness (EET). Violet and red contours with labels show the EET values from Audet and Bürgmann (2011) and Chen et al. (2015), respectively. Continuous black contours show state boundaries. The dashed black contour shows the boundary between the Arabian Shield and Platform. White circles show the earthquake locations.

of the Arabian shield. In the East, the Arabian Plate is bounded by the Zagros fold belt where numerous large earthquakes are generated, consequently to the compressional forces acting in the collision zone (e.g., Al-Amri et al., 2016). On the other hand, only very moderate seismicity characterizes the inner part of the Arabian Plate with no clear relationship with the boundary between the Shield and Platform. This fact gives some preference to Model II, which indicates that Arabian Plate is affected by very little internal deformation, being almost entirely characterized by large values of strength (>1.5–2 10^{13} Pa m).

The results of the rheological approach used to estimate the lithospheric strength and effective elastic thickness are substantially different from previous studies that were based on a cross-spectral analysis of the gravity field and surface load. Recent estimates of the EET in this region, obtained using the fan wavelet method (Chen et al., 2015), predicted relatively low (10–30 km) and high (>50 km) values in the Shield and Platform, respectively (Figs.9c and 10c). Previous regional and global studies, based on the spectral coherence analysis of topography and Bouguer anomaly data, have shown similar variations in EET (Audet and Bürgmann, 2011), or in some cases even stronger, predicting values larger than 100 km in the central part of the Platform (Pérez-Gussinyé et al., 2009). In contrast, in both Model I and Model II the variations of the EET across the plate are sharper, and the main variation is shifted to the west (Figs. 9c and 10c). The large difference in the rigidity between the Shield and Platform is clearly observed in Model I from the bimodal distribution of the EET around the two main peaks at 40 km (8%) and 70 km (17%), respectively (Fig. 11a). In contrast, in Model II this difference is not evident, since the values are distributed around one main peak at 80 km (20%) (Fig. 11b). The estimates of Chen et al. (2015) are significantly lower, distributed only around the main peak at 15 km (15%) (Fig. 11a and b). Furthermore, Chen et al. (2015) estimated the largest values of the EET (>80 km) in the central part of the Platform, while farther to the east the EET decreases to ~45 km. However, our results may be overestimated in the eastern Platform (~100 km), since the final densities decrease more significantly in the shallowest mantle (~0.04 g/cm^3) than at a depth of 100 km (~0.02 g/cm^3) (Fig. 5a). Therefore, the temperatures in the uppermost mantle may be larger by ~50–70 °C than those estimated from the linear interpolation (Fig. 5b, cross-sections A-A′ and B-B′). This would lead to a reduction in the EET by 10–15 km. Thus, the values would be similar to those for the central Arabian Plate, in agreement with the results of regional seismic tomography, also predicting a thick cold lithosphere in the eastern platform (Koulakov et al., 2016; Priestley et al., 2012). The values < 50 km, as those obtained by Chen et al. (2015), would suggest the near total absence of the MSUM, which is unlikely in these regions.

5. Conclusions

1. We constructed a thermal model of the Arabian Plate by using crustal geotherms constrained by heat flow measurements. The thermal model of the mantle is based on seismic tomography corrected for the density variations estimated in a joint inversion with the residual mantle gravity field and residual topography. The constructed

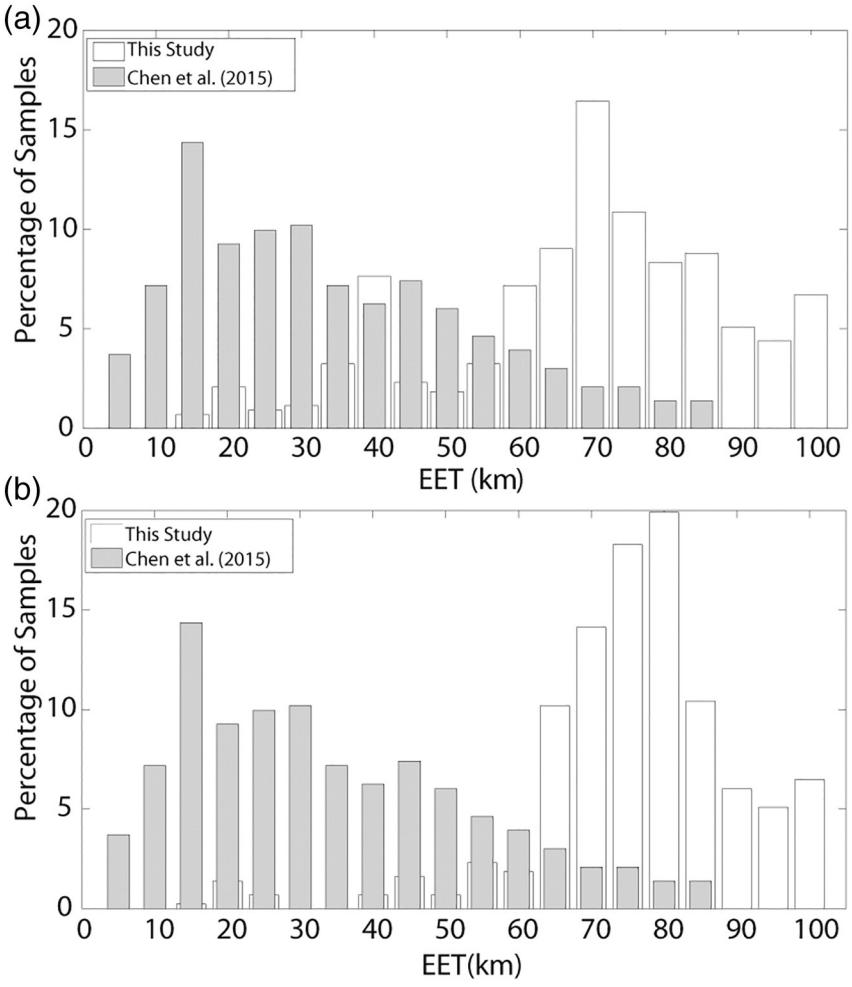

Fig. 11. Bar plots of the EET estimated (a) using a uniform value for the strain rates (in white) and from the study of Chen et al. (2015) (in grey); (b) using variable values for the strain rates in both horizontal and vertical directions (in white) and from the study of Chen et al. (2015) (in grey).

thermal model shows sharp variations in the uppermost mantle from the hot Arabian Shield to the cold Arabian Platform. However, this difference is decreased to 100–200 °C below a depth of 100 km.

2. The new thermal model and the crustal model of Kaban et al. (2016b) provide inputs for the strength and EET estimation. Based on these data we construct two alternative models. In Model I, a constant value of the strain rates is used, while Model II includes variable strain rates both in the horizontal and vertical direction, obtained from a recent global mantle flow model. We found that the spatially variable strain rates significantly affect the calculated strength and EET of the lithosphere, shifting the transition from low to high rigidity, characterizing the Arabian Shield and Platform from the boundary of these features toward the central part of the Shield, respectively.
3. Although both Model I and Model II show that the strength is predominantly concentrated in the crust throughout the entire study area, the thickness of the mechanically strong upper mantle (MSUM) is relatively large (up to ~50 km) in the Arabian platform, ensuring its long-term stability.
4. The difference in the coupling/decoupling conditions of the crust from the upper mantle causes a more significant and sharper eastward increase in the EET from 40 km to 70 km close to the boundary between the Shield and Platform in Model I, while in Model II large values of EET are extended to most of the Shield. Furthermore, the largest EET estimates (≥70 km) are not confined to the central Platform as in the previous study of Chen et al. (2015), which was based on spectral gravity methods, but are representative of the majority of this tectonic feature.

Acknowledgments

This study was funded by, Utrecht University, and the Netherlands Research Centre for Integrated Solid Earth Science (ISES-2014-UU-08, ISES-2016-UU-19). A.G.P. was supported by the German Research Foundation (grant PE 2167/1-1). The authors extend their appreciation to the International Scientific Partnership Program ISPP for funding this research work through ISPP#0052. Comments from the Editor Philippe Agard and two anonymous reviewers helped to improve the manuscript.

References

Al-Amri, A., Abdelrahman, K., Andreae, M.O., Al-Dabbagh, M., 2016. Crustal and upper mantle structure beneath the Arabian Shield and Red sea. In: Roure, F., Amin, A., Khomsi, S., Al Garni, M. (Eds.), Lithosphere Dynamics and Sedimentary Basins of the Arabian Plate and Surrounding Areas. Springer (in press).

Argus, D.F., Gordon, R.G., DeMets, C., 2011. Geologically current motion of 56 plates relative to the no-net-rotation reference frame. Geochem. Geophys. Geosyst. 12 (11).

ArRajehi, A., McClusky, S., Reilinger, R., Daoud, M., Alchalbi, A., Ergintav, S., Kogan, L., 2010. Geodetic constraints on present-day motion of the Arabian Plate: implications for Red Sea and Gulf of Aden rifting. Tectonics 29 (3), TC3011.

Audet, P., Bürgmann, R., 2011. Dominant role of tectonic inheritance in supercontinent cycles. Nat. Geosci. 4:184–187. http://dx.doi.org/10.1038/NGEO1080.

Burov, E.B., Diament, M., 1995. The effective elastic thickness (*Te*) of continental lithosphere. What does it really means? J. Geophys. Res. 100, 3895–3904.

Byerlee, J., 1978. Friction of rocks. Pure Appl. Geophys. 116 (4–5), 615–626.

Cammarano, F., Goes, S., Vacher, P., Giardini, D., 2003. Inferring upper-mantle temperatures from seismic velocities. Phys. Earth Planet. Inter. 138:197–222. http://dx.doi.org/10.1016/S00319201(03)00156-0.

Camp, V., Roobol, M., 1992. Upwelling asthenosphere beneath western Arabia and its regional implications. J. Geophys. Res. 97, 15255–15271.

Carter, N.L., Tsenn, M.C., 1987. Flow properties of continental lithosphere. Tectonophysics 136, 27–63.

Chang, S.-J., Merino, M., Van der Lee, S., Stein, S., Stein, C.A., 2011. Mantle flow beneath Arabia offset from the opening Red Sea. Geophys. Res. Lett. 38, L04301. http://dx.doi.org/10.1029/2010GL045852.

Chen, B., Kaban, M.K., El Khrepy, S., Al-Arifi, N., 2015. Effective elastic thickness of the Arabian Plate: weak shield versus strong platform. Geophys. Res. Lett. 42. http://dx.doi.org/10.1002/2015GL063725.

Christensen, N.I., Mooney, W.D., 1995. Seismic velocity structure and composition of the continental crust: a global review. J. Geophys. Res. 100, 9761–9788.

Demouchy, S., Tommasi, A., Boffa-Ballaran, T., Cordier, P., 2013. Low strength of Earth's uppermost mantle inferred from tri-axial deformation experiments on dry olivine crystals. Phys. Earth Planet. Inter. 220, 37–49.

Förster, H.J., Förster, A., Oberhansli, R., Stromeyer, D., 2010. Lithospheric composition and thermal structure of the Arabian Shield in Jordan. Tectonophysics 481:29–37. http://dx.doi.org/10.1016/j.tecto.2008.1011.1014.

François, T., Burov, E.B., Meyer, B., Agard, P., 2013. Surface topography as key constraint on thermo-rheological structure of stable cratons. Tectonophysics 602, 106–123.

Galanis, S.P., Sass, J.H., Munroe, R.J., Abu-Ajamieh, M., 1986. Heat flow at Zerqa Ma'in and Zara and a geothermal reconnaissance of Jordan. US Geological Survey, Open File Report. 86–63 (Menlo Park).

Gettings, M.E., Blank, H.R., Mooney, W.D., Healey, J.H., 1986. Crustal structure of southwestern Saudi Arabia. J. Geophys. Res. 91, 6491–6512.

Goetze, C., Evans, B., 1979. Stress and temperature in the bending lithosphere as constrained by experimental rock mechanics. Geophys. J. Int. 59, 463–478.

Griffin, W.L., O'Reilly, S.Y., Abe, N., Aulback, S., Davies, R.M., Pearson, N.J., Doyle, B.J., Kivi, K., 2003. The origin and evolution of Archean lithospheric mantle. Precambrian Res. 127, 19–41.

Hansen, S.E., Gaherty, J.B., Schwartz, S.Y., Rodgers, A.J., Al-Amri, A.M.S., 2008. Seismic velocity structure and depth-dependence of anisotropy in the Red Sea and Arabian shield from surface wave analysis. J. Geophys. Res. 113, B10307. http://dx.doi.org/10.1029/2007JB005335.

Hasterok, D., Chapman, D.S., 2011. Heat production and geotherms for the continental lithosphere. Earth Planet. Sci. Lett. 307, 59–70.

Jackson, J., 2002. Strength of the continental lithosphere: time to abandon the jelly sandwich? GSA Today 12 (9), 4–9.

Kaban, M.K., Petrunin, A.G., Schmeling, H., Shahraki, M., 2014. Effect of decoupling of lithospheric plates on the observed geoid. Surv. Geophys. 35:1361–1373. http://dx.doi.org/10.1007/s10712-014-9281-3.

Kaban, M.K., Mooney, W.D., Petrunin, A.G., 2015. Cratonic root beneath North America shifted by basal drag from the convecting mantle. Nat. Geosci. http://dx.doi.org/10.1038/ngeo2525.

Kaban, M.K., El Khrepy, S., Al-Arifi, N., Tesauro, M., Stolk, W., 2016a. 3D density model of the upper mantle in the Middle East: interaction of diverse tectonic processes. J. Geophys. Res. 121. http://dx.doi.org/10.1002/2015JB012755.

Kaban, M.K., El Khrepy, S., Al-Arifi, N., 2016b. Isostatic model and isostatic gravity anomalies of the Arabian Plate and surroundings. Pure Appl. Geophys. 173 (4):1211–1221. http://dx.doi.org/10.1007/s00024-015-1164-0.

Karato, S.-I., Jung, H., 2003. Effects of pressure on high-temperature dislocation creep in olivine. Philos. Mag. A 83, 401–414.

Koulakov, I., Burov, E., Cloetingh, S., El Khrepy, S., Al-Arifi, N., Bushenkova, N., 2016. Evidence for anomalous mantle upwelling beneath the Arabian Platform from travel time tomography inversion. Tectonophysics 667, 176–188.

Kreemer, C., Blewitt, G., Klein, E.C., 2014. A geodetic plate motion and global strain rate model. Geochem. Geophys. Geosyst. 15 (10), 3849–3889.

Laske, G., Masters, G., Ma, Z., Pasyanos, M., 2013. Update on CRUST1.0 — a 1-degree globalmodel of Earth's crust. Geophys. Res. Abstr. 15 (Abstract EGU2013-2658, 2013).

McDonough, W.F., Sun, S.-S., 1995. The composition of the Earth. Chem. Geol. 120, 223–253.

McGuire, A.V., Bohannon, R.G., 1989. Timing of mantle upwelling: evidence for a passive origin for the Red Sea Rift. J. Geophys. Res. 94, 1677–1682.

Mooney, W.D., Ritsema, J., Hwang, Y.K., 2012. Crustal seismicity and the earthquake catalog maximum moment magnitude (M cmax) in stable continental regions (SCRs): correlation with the seismic velocity of the lithosphere. Earth Planet. Sci. Lett. 357, 78–83.

Mooney, W.D., 2014. Global crustal structure. In: Romanowicz, B., Dziewonski, A. (Eds.), Crust and Mantle, second edition vol. 1. Elsevier, Netherlands (volume editors, G.Schubert, Treatise editor-in-Chief).

O'Reilly, S.Y., Griffin, W.L., 2012. Mantle metasomatism. In: Harlov, D.E., Austrheim, H. (Eds.), Metasomatism and the Chemical Transformation of Rock. Lecture Notes in Earth System Sciences. Springer-Verlag, Berlin Heidelberg:pp. 467–528 http://dx.doi.org/10.1007/978-3-642-28394-9_12.

Park, Y., Nyblade, A.A., Rodgers, A.J., Al-Amri, A., 2007. Upper mantle structure beneath the Arabian Peninsula and northern Red Sea from teleseismic body wave tomography: implications for the origin of Cenozoic uplift and volcanism in the Arabian Shield. Geochem. Geophys. Geosyst. 8:Q06021. http://dx.doi.org/10.1029/2006GC001566.

Paulson, A., Zhong, S., Wahr, J., 2005. Modelling post-glacial rebound with lateral viscosity variations. Geophys. J. Int. 163 (1), 357–371.

Pérez-Gussinyé, M., Metois, M., Fernández, M., Vergés, J., Fullea, J., Lowry, A.R., 2009. Effective elastic thickness of Africa and its relationship to other proxies for lithospheric structure and surface tectonics. Earth Planet. Sci. Lett. 287, 152–167.

Petrunin, A.G., Kaban, M.K., Rogozhina, I., Trubitsyn, V., 2013. Revising the spectral method as applied to modeling mantle dynamics. Geochem. Geophys. Geosyst. (G3) (EDOC: 21048).

Priestley, K., McKenzie, D., Barron, J., Tatar, M., Debayle, E., 2012. The Zagros core: deformation of the continental lithospheric mantle. Geochem. Geophys. Geosyst. 13 (11).

Ranalli, G., 1994. Nonlinear flexure and equivalent mechanical thickness of the lithosphere Tectonophysics. 240 pp. 107–114.

Ritsema, J., Deuss, A., van Heijst, H.J., Woodhouse, J.H., 2011. S40RTS: a degree-40 shear-velocity model for the mantle from new Rayleigh wave dispersion, teleseismic traveltime and normal-mode splitting function measurements. Geophys. J. Int. 184 (3), 1223–1236.

Rolandone, F., Lucazeau, F., Leroy, S., Mareschal, J.-C., Jorand, R., Goutorbe, B., Bouquerel, H., 2013. New heat flow measurements in Oman and the thermal state of the Arabian Shield and Platform. Tectonophysics 589, 77–89.

Schaeffer, A.J., Lebedev, S., 2013. Global shear-speed structure of the upper mantle and transition zone. Geophys. J. Int. 194, 417–449.

Steinberger, B., Calderwood, A.R., 2006. Models of large-scale viscous flow in the Earth's mantle with constraints from mineral physics and surface observations. Geophys. J. Int. 167, 1461–1481.

Stern, R.J., Johnson, P., 2010. Continental lithosphere of the Arabian Plate: a geologic, petrologic, and geophysical synthesis. Earth Sci. Rev. 101, 29–67.
Stixrude, L., Lithgow-Bertelloni, C., 2005. Thermodynamics of mantle minerals – I. Physical properties. Geophys. J. Int. 162, 610–632.
Stolk, W., Kaban, M.K., Beekman, F., Tesauro, M., Mooney, W.D., Cloetingh, S., 2013. High resolution regional crustal models from irregularly distributed data: application to Asia and adjacent areas. Tectonophysics 602, 55–68.
Tesauro, M., Audet, P., Kaban, M.K., Bürgmann, R., Cloetingh, S.A.P.L., 2012a. The effective elastic thickness of the continental lithosphere: comparison between rheological and inverse approaches. Geochem. Geophys. Geosyst. 13, Q09001. http://dx.doi.org/10.1029/2012GC004162.
Tesauro, M., Kaban, M.K., Cloetingh, S.A.P.L., 2012b. Global strength and elastic thickness of the lithosphere. Glob. Planet. Chang. 90–91:51–57. http://dx.doi.org/10.1016/j.gloplacha.2011.12.003.
Tesauro, M., Kaban, M.K., Cloetingh, S.A.P.L., 2013. Global model for the lithospheric strength and effective elastic thickness. Tectonophysics 602, 78–86.
Tesauro, M., Kaban, M.K., Mooney, W.D., 2015. Variations of the lithospheric strength and elastic thickness in North America. Geochem. Geophys. Geosyst. 16. http://dx.doi.org/10.1002/2015GC005937.
Wilks, K.R., Carter, N.L., 1990. Rheology of some continental lower crustal rocks. Tectonophysics 182, 57–77.